Lower Murray Reclaimed Irrigation Area (LMRIA) Acidification Project

A biogeochemical model for assessing and managing acid sulfate soils in the Lower Murray region of South Australia

ALTERRA
WAGE INGEN UR

EPA
South Australia

Lower Murray Reclaimed Irrigation Area (LMRIA) Acidification Project

A biogeochemical model for assessing and managing acid sulfate soils in the Lower Murray region of South Australia

Authors: Luke M Mosley[A,B], Rob Fitzpatrick[B] and Bert-Jan Groenenberg[C]

[A] Environment Protection Authority, Adelaide

[B] AcidSulfate Soils Centre, The University of Adelaide

[C] AlterraWageningenUR, PO. Box 47, 6700 AA, The Netherlands

For further information please contact:

Information Officer
Environment Protection Authority
GPO Box 2607
Adelaide SA 5001

Telephone: (08) 8204 2004
Facsimile: (08) 8124 4670
Free call (country): 1800 623 445

Website: <www.epa.sa.gov.au>

Email: <epainfo@epa.sa.gov.au>

Cover picture: clockwise from right, a soil profile showing presence of acid sulfate soil minerals, acidified drain water with visible orange-brown (Schwertmannite precipitates) and drain pumping into the River Murray(EPA & CSIRO)

ISBN 978-1-921495-51-9

July 2014

This project was funded by the Murray–Darling Basin Authority, Canberra, Australia.

Contents

List of figures

List of tables

Abbreviations

CSIRO	Commonwealth Scientific and Industrial Research Organisation
EPA	South Australian Environment Protection Authority
LMRIA	Lower Murray Reclaimed Irrgiation Area
SMASS	Simulation Model for Acid Sulfate Soils

Summary

Acid sulfate soils and acid mine drainage pose significant management challenges and risks to the environment. Application of modelling to acid sulfate soils has been limited. Geochemical modeling could potentially be very useful in predicting and managing acid sulfate soil impacts and processes (eg pyrite oxidation under different hydrological conditions, metal release and export, recovery timescales).

Drought conditions and low inflows from 2006 to early 2010 in the Murray–Darling system in Australia led to unprecedented low water levels in the lower reaches of the river below Lock 1. This resulted in groundwater tables falling below the adjacent agricultural areas known as the Lower Murray Reclaimed Irrigation Area or LMRIA. The heavy clay soils subsequently salinised, dried and cracked, resulting in pyrite oxidation of previously waterlogged, anaerobic hypersulfidic material approximately 1–3 m below ground level (bgl).

The return of river and groundwater levels in late 2010 resulted in the appearance of acid drainage across an area of 3,300 ha and resultant river water quality risks. There was a critical need to better quantify and model the biogeochemical processes in the LMRIA subsoils to improve risk management and to be able to evaluate mitigation measurements for acidified soils.

An existing multilayer biogeochemical model (SMARTml model) was modified to include a pyrite oxidation model that is based on the Simulation Model for Acid Sulfate Soils (SMASS). SMARTml was also modified so it could receive inputs from the widely used Hydrus-1D soil hydrology model. This coupled SMARTml model enabled simulation of pyrite oxidation, metal speciation, and other complex biogeochemical processes in acid sulfate soils.

The pyrite oxidation model was developed and tested at the Long Flat irrigation area in the LMRIA. An extensive soil and groundwater data set (series of multilevel piezometers) was used to parameterise and test the SMARTml model performance. Measured soil physical properties were used to parameterise the Hydrus-1D model. The Hydrus-1D model was calibrated and successfully represented current wetting and drying cycles at the site. Regional groundwater data was used to simulate the falling water table under the LMRIA during the 2007–09 drought in Hydrus-1D.

The predicted water contents from the Hydrus-1D model decreased markedly during drought and indicated soil drying would occur to a depth of up to 3 m below ground level. This was consistent with the oxidized zone of sulfuric material (pH<4) and reactive metal fractions in the LMRIA subsoil layers. The soil pH profile, and depth and severity of pyrite oxidation were successfully simulated in SMARTml over a 1,850-day period. The model also successfully represented the flushing of solutes from the soil profile and solution metal concentrations once irrigation recommenced in the LMRIA.

The development of the model provided a useful management tool for assessing and managing impacts from acid sulfate soils. For the LMRIA, preliminary management scenarios demonstrated how maintaining desirable river levels (>0.5 m AHD which corresponds to the Basin Plan guideline of maintaining downstream Lower Lakes levels >0.4 m AHD, 95% of the time) is critical to preventing oxidation of hypersulfidic material in acid sulfate soils.

Further testing and development of SMARTml (to include sulfate reduction) would be beneficial. The reactivity of carbon in the deeper subsoils should also be assessed to refine the oxygen consumption parameter in the model and to inform on the lability of this carbon for sulfate reduction. Additional modeling using a two-dimensional model to couple river level to groundwater level under the floodplain would also be worthwhile for refining management outcomes.

1 Introduction

Acid sulfate soils are the common name given to sediments and soils containing iron sulfides (typically pyrite FeS2) which, when exposed to oxygen, generate products of sulfide oxidation such as sulfuric acid (Pons 1973, Dent and Pons 1995). These soils form naturally in the presence of iron-rich sediments, sufficient sulfate and plentiful supply of organic matter. Such conditions commonly exist in mangroves, wetlands, salt marsh vegetation or tidal areas, and at the bottom of coastal rivers and lakes. Left waterlogged, materials in acid sulfate soils may remain inert and reduced in the form of sulfidic or hypersulfidic material (pH >4).

However, drainage and disturbance of hypersulfidic material can result in oxidation and the subsequent formation of sulfuric material with high levels of acidity (pH <4) and soluble metals (Dent and Pons 1995, Fitzpatrick *et al* 2013). The acid and metals arising from sulfuric material are stored in pore-waters and may be transported into water bodies as the hypersulfidic material drains or rewets, and this can lead to severe ecological effects. Oxidised sulfuric material in acid sulfate soils can also export acidity and solutes for long periods of time.

The biogeochemistry of acid sulfate soils is complex (Dent and Pons 1995), involving oxygen transport into the sediment (required to oxidise pyrite), kinetic controlled reactions (eg pyrite oxidation, dissolved iron reactions), secondary acidification effects (eg acidic mineral formation, metal solubilisation), transport processes (eg leaching, diffusion to surface and ground water), and acid neutralisation reactions (eg sulfate reduction, carbonate dissolution).

Currently, there is no single model available that can adequately simulate all the potential processes influencing the biogeochemistry of acid sulfate soils. However, some models have been developed for oxidation and leaching processes of pyrite in mining contexts (Wunderly *et al* 2006).

The Simulation Model for Acid Sulfate Soils (SMASS) developed by Bronswijk and Groenenberg (1992) incorporates most relevant processes but does not include many potentially important and more recently researched aspects (eg ion binding to dissolved and solid organic matter, clays and oxides). Recently a multilayer soil process model (SMARTml) has been developed for simulation of acidification and transport of nutrients and trace elements in soil that includes these processes (Bonten *et al* 2011). By incorporating the SMASS acid sulfate soil model functionality into the SMARTml model the biogeochemistry of acid sulfate soils could be better assessed. This would enable improved risk assessment and management of the impacts of acid sulfate soils.

Drought conditions and low inflows from 2006 to early 2010 in the Murray–Darling system in Australia led to unprecedented low water levels in the lower reaches of the river below Lock 1 at Blanchetown, South Australia. This resulted in groundwater tables falling under the adjacent agricultural areas of the Lower Murray Reclaimed Irrigation Area or LMRIA. The heavy clay soils subsequently salinised, dried and cracked, resulting in pyrite oxidation of previously waterlogged, anaerobic hypersulfidic material approximately 1–3 m below ground level (bgl) [see Fitzpatrick *et al* 2013]. The return of the river to normal pool levels and subsequent recovery of groundwater levels in late 2010 resulted in the appearance of acid drainage across an area of 3,300 ha and resultant river water quality risks. There was a critical need to better quantify and model the biogeochemical processes in the LMRIA subsoil layers to improve risk management and to be able to evaluate mitigation measurements for acidified soils.

The aims of this study were to:

- describe the development of a new 1 dimensional (1D) biogeochemical model framework for acid sulfate soils
- apply the model to simulate acid generation and drainage processes in an agricultural area in the Lower Murray River region of South Australia.

2 Methods

An outline of the model framework is shown in Figure 1.

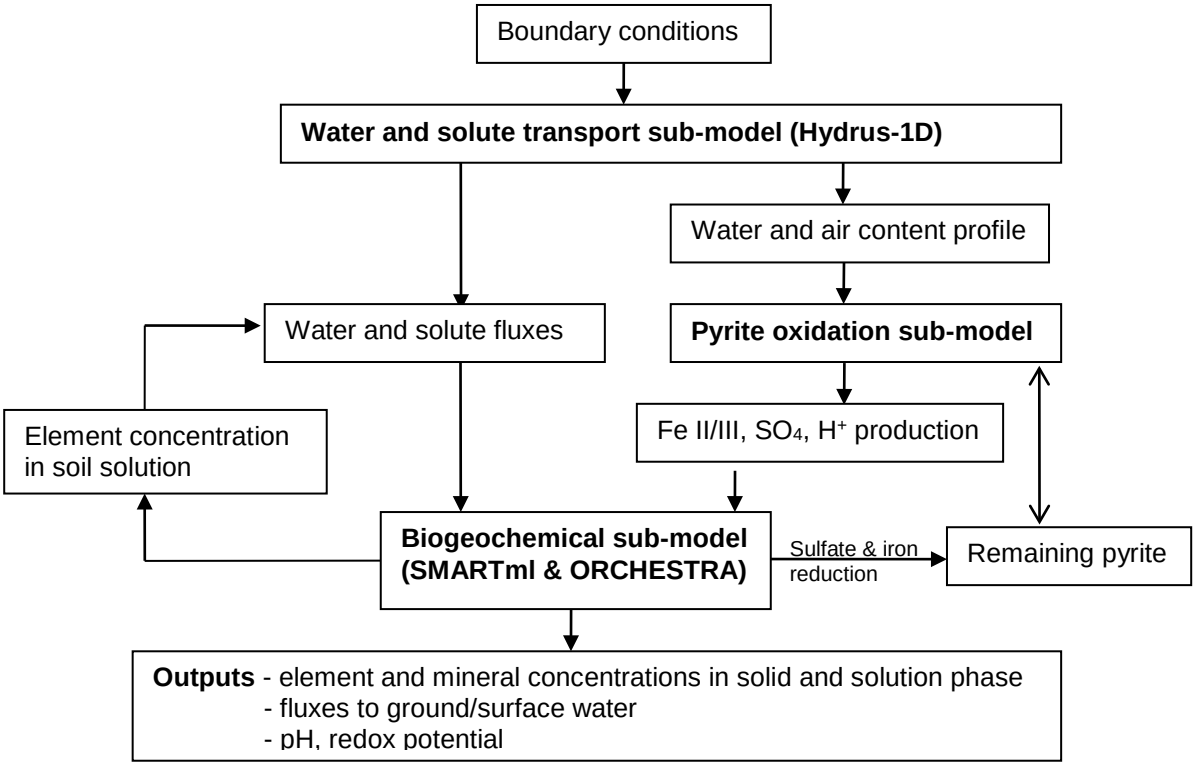

Figure 1 Model framework

The following various sub-models were coupled together (independently) to create a 1D model framework for simulating acid sulfate soil biogeochemical reactions and transport processes:

Water and solute transport sub-model

The widely used and supported model for water and solute flows in variably saturated media, Hydrus-1D, was used to provide moisture content and fluxes at various depths/compartments in the soil profile. HYDRUS's Graphical User Interface enables schematisation of the soil profile, and defining of different top and bottom boundary conditions and hydraulic properties (Figure 2). Comprehensive details on the Hydrus-1D model can be found in Simunek *et al* (2008) and on the Hydrus/PC Progress website.

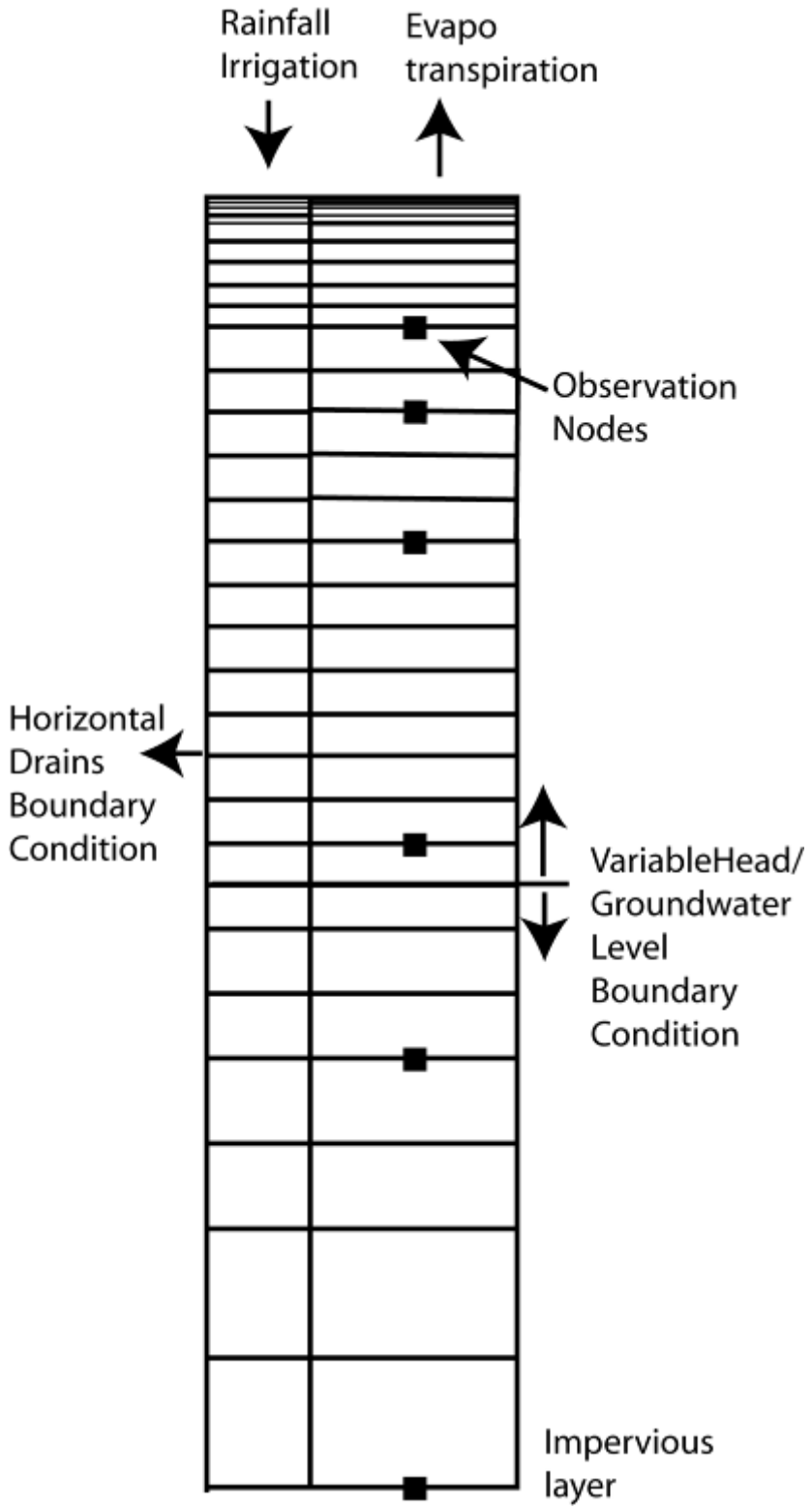

Figure 2 Schematic diagram of Hydrus-1D model components

Biogeochemical sub-model

The basis of the biogeochemical sub-model is the SMARTml model (Bonten *et al* 2011) , a multi-layer soil process model originally developed to simulate soil acidification, nutrient cycling and the fate of trace elements in response to changes in atmospheric deposition. The model includes (i) atmosphere-plant interactions, (ii) plant uptake of macro- and trace elements, (iii) biochemical processes including soil organic matter mineralisation, nitrification and denitrification and (iv)

geochemical processes, including mineral weathering and ion binding of macro-ions (egCa, Al, S) and trace elements (eg As, Zn) to organic matter, clay and iron and aluminum oxides.

Furthermore the model includes the chemical speciation of the elements in solution. Equilibrium reactions are calculated using the ORCHESTRA biogeochemical model (Meeussen *et al* 2003). The model was extended with oxidation and reduction processes important for acid sulfate soilsie pyrite oxidation, oxidation and reduction of iron and sulfur. In the present application, plant-atmosphere interactions and plant uptake were neglected.

The model includes the following macro-elements: Ca, Mg, K, Na, Cl, SO_4,PO_4, S(II), NO_3, NH_4, Fe(III), Fe(II) and Al. Ion exchange reactions of trace elements are included and parameterised for a large set of trace elements (Dijkstra *et al* 2009, Groenenberg *et al* 2012) but not (yet) included in the present application of the model.

Changes in concentrations of all elements follow the general differential balance equation:

$$\frac{d(\theta_n \cdot z_n \cdot cX_n + \rho_n \cdot z_n \cdot QX_n)}{dt} = X_{in,n} + \Phi_{out,n-1} \cdot cX_{n-1} - \Phi_{out,n} \cdot cX_n \quad (1)$$

Where, cX_n is the concentration of element X in layer n (eq m–3); θ_n is the moisture content (m3·m–3); z_n is the height of model layer n (m); ρ_n is the bulk density (kg·m–3); QX_n is the solid phase (sorbed or mineral) content of element X (eq kg–1); $X_{in.n}$is the total input to a soil layer (eq·yr-1); $\Phi_{out,n}$ is the outgoing water flux and influx for the next layer (m·yr–1). The concentration of protons is calculated from the charge balance of all considered elements.

This equation is discretised as:

$$z_n \cdot (\theta_{n,t} \cdot cX_{n,t} - \theta_{n,t-\Delta t} \cdot cX_{n,t-\Delta t}) + \rho_n \cdot z_n \cdot (QX_{n,t} - QX_{n,t-\Delta t}) = (X_{in,n,t} + \Phi_{out,n-1,t} \cdot cX_{n-1,t} - \Phi_{out,n,t} \cdot cX_{n,t}) \cdot \Delta t \quad (2)$$

Where, Δt is the time step size (day).

Carbon and nitrogen processes

Mineralisation of C and N is modeled similarly as in the model VSD+ (Bonten *et al* 2009). Here, organic C is assumed to consist of four pools, each with a fixed C:N ratio, a first order decomposition rate (kref) and a fixed ratio between mineralisation and turnover to a next C pool (frhu). The first two pools contain fresh litter from both litterfall and root decay. Decomposition of these two pools leads to mineralisation of C and N (ie NH_4 formation), and turnover to a third pool. Decomposition of the third pool leads to mineralisation and turnover to the last pool, which can only be mineralised. Decomposition rates are described as reference rates which are modified for environmental factors, ie temperature, moisture and pH.

Weathering

Weathering is calculated using a zero order rate constant which is pH dependent.

$$X_{we} = kX_{we} \cdot z \cdot cH^{coefHwe} \cdot \Delta t \quad (3)$$

where kX_{we} is the weathering rate (eq/m2/yr) and X is Ca, Mg, K and Na, coefHwe is the coefficient for pH dependent weathering.

Aluminium weathering is proportional to weathering of base cations:

$$kAl_{we} = rat \cdot (kCa_{we} + kMg_{we}) \quad (4)$$

Iron and sulfate reduction

The model is prepared to include sulfate and iron reduction, however rate constants are still to be derived and this process was therefore not yet included in the present model application.

In the absence of oxygen and nitrate both ferric iron and sulfate are reduced within the model using a first order rate constant:

$$X_{re} = kX_{re}.X.z.\Delta t \quad (5)$$

where kX_{re} is the reduction rate (eq/m^2/yr) and X_{re} is reactive SO_4 or Fe(III).

Chemical equilibria

After the calculation of the kinetic reactions described above the total concentrations of each chemical component were calculated in allsoil layers by summing the production/consumption terms, and inflow/outflow fluxes by solute transport, and the total amounts from the previous time step according to Equation 2.

From these total concentrations, the equilibrium concentrations in the soil solution and the soil solid phase (adsorbed ions and mineral precipitates) were computed for each compartment using the model ORCHESTRA according to the set up and parameterisation of Bonten *et al* (2011). Additionally to the setup of Bonten *et al* (2011) we included the reduced species Fe(II) and S(II) which are both modeled as independent chemical entities, ie. within ORCHESTRA we do not consider redox reactions of Fe and S.

ORCHESTRA includes the NICA-Donnan model (Kinniburgh *et al* 1990) for ion binding to soil organic matter and dissolved organic matter, the generalised two layer model (Dzombak and Morel 1990)for ion binding to Al and Fe (hydr)oxides and a Donnan model for electrostatic binding to clay minerals, according to the setup of Bonten *et al*(2011). For ion binding to organic matter in the NICA-Donnan model parameters of Milne *et al* (2003,2004) except for the binding of Fe^{3+} for which we used the parameters of Hiemstra and van Riemsdijk (2006) were used.

For ion binding to Al and Fe oxides the parameters by Dzombak and Morel (1990) were used. Inorganic complexation in the solution phase and mineral equilibria were calculated using the MINTEQA2 database (Allison *et al* 1991).We considered the precipitates/minerals ferric hydroxide, gibbsite, jarosite (both K-jarosite and Na-jarosite) and schwertmannite.

Oxygen diffusion and pyrite oxidation sub-model

Under aerobic conditions the rate of pyrite oxidation is dependent on the transport rate of oxygen towards the pyrite. To calculate oxygen transport we used the oxygen diffusion and pyrite oxidation model of Bronswijk and Groenenberg (Bronswijk and Groenenberg 1992, Bronswijk*et al* 1993), which was developed for structured (clay) soils. The model includes oxygen diffusion through macro-pores and diffusion into soil aggregates. Oxygen is consumed inside the soil aggregates by organic matter mineralization and pyrite oxidation.

Organic matter mineralisation is largely independent of the O_2 concentration in the soil and modeled with a constant oxygen consumption rate (kg O_2/kg OM). Pyrite oxidation is calculated using a shrinking core diameter model with a rate constant for pyrite oxidation according to:

$$K = 0.051877\sqrt{C_w} \quad (5)$$

in which K = oxidation rate of pyrite by dissolved O_2 (kg.m^{-2}.d^{-1}) and C_w = the concentration of dissolved O_2 (kg.m^{-3}). For each time-step the model solves the steady state oxygen profile based on the air filled porosity (air filled porosity= total porosity – water content) calculated with Hydrus-1D. Pyrite oxidation products (Fe III, SO_4, H^+) in each soil compartment are calculated according to the following reaction:

FeS2 + 3 ¾ O2 + ½ H2O → Fe3+ + 2SO4 + H+ (6)

3 Model application example in the LMRIA

The coupled model described earlier was applied to simulate the pyrite oxidation processes; acid production and buffering (cation exchange, weathering), the production of retained acidity (Jarosite), mobilisation of acidic cations (H^+, Al III, Mn II, Fe II/III), trace elements (As, Ni) and nutrients, in the Long Flat irrigation area in the LMRIA region (Figure 3) using soil and water data sets collected at this site.

The model was run for the period 2007-2012. This period included the drawdown of the water table (2007–09) the rise of the water table (2010) and a period of several irrigation events (2011–12). For the hydrological and biogeochemical model the soil column until 3–m depth was discretised to 30 nodes for the hydrological model and 29 soil layers in SMARTml.

Model inputs

Hydrology

A push-tube corer was used to collect soil cores to a depth of 3 m at three sites in June 2011 and April 2012 (see Fitzpatrick *et al* 2013) with the results from the middle site B (see Figure 3) used for modeling purposes. Wet soil samples were analysed for a range of parameters including pH in water (using a calibrated pH electrode), bulk density (gravimetric method), particle size (% sand, silt, clay by hydrometer method from Gee and Bauder 1986). Particle size and bulk density results were used in pedotransfer functions (Rawls and Brakensiek 1985) to calculate the hydraulic parameters used in the Hydrus-1D model shown in Table 1.

River level (Site 4261003) and groundwater levels (Mobilong Site 1A) were obtained from the Department for Environment, Water and Natural Resources South Australia. The groundwater level was used as the bottom boundary condition in Hydrus for the water level drawdown and refill period.

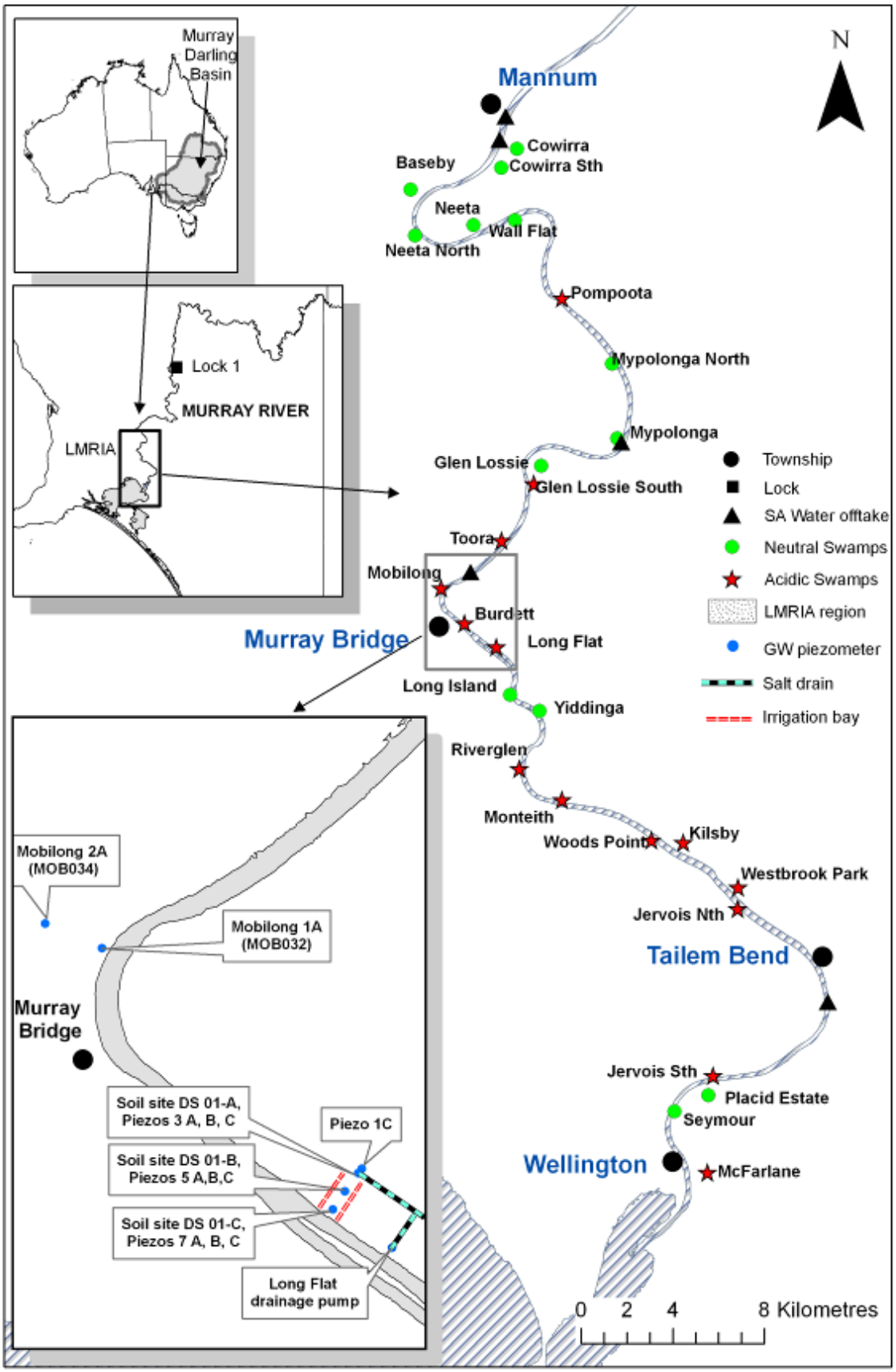

Figure 3 **The Lower Murray Reclaimed Irrigation Area (LMRIA) region in the lower River Murray of South Australia showing location of acidic and neutral swamps. The inset map shows the location of soil and groundwater monitoring stations at Long Flat and Mobilong.**

Table 1 **Soil physical and hydraulic properties used in the Hydrus-1D model, where θ_r is the residual water content [L^3L^{-3}]; $\theta_s$is the saturated water content [L^3L^{-3}]; α and n are empirical shape parameters in the soil water retention function; K_s is the saturated hydraulic conductivity [LT^{-1}]; l is the tortuosity parameter in the conductivity function; and Bulk D. is the soil bulk density.**

Layer	Depth (m)	θ_r	θ_s	α	*n*	K_sm/day	l	Bulk D.
1	0–1	0.10	0.587	3.947	1.537	1.3	0.5	1.09
2	1–3	0.10	0.590	2.117	1.709	0.1/1.3*	0.5	1.09

* The saturated hydraulic conductivity in layer 2 was increased from 0.1 m/day to 1.3 m/day (same as upper layer) once the deeper (<1m) soil profile had dried (post day 1000).

Initial soil chemical properties

Sub-samples of soil from the Long Flat irrigation area were dried (at 60°C for 48hrs) prior to crushing and analysis for total metals (1:1 Nitric/HCl digest – APHA method 3125 ICPMS, exchangeable bases (using standard Ammonium Acetate extract APHA Method 15D3 with no pretreatment for soluble salts), and full acid-base characteristics including pyrite by the Chromium reducible sulfur technique (Method 22B from Ahern *et al* 2004).

Initial soil properties used in the SMARTml model are shown in Table 2. These are based on the measurements in 2011 and 2012 of the soil organic matter content, clay content, bulk density, pyrite content (Cr-reducible sulfur), reactive iron and aluminium (the sum of the $MgCl_2$, HCl and Na-pyrophosphate extraction) and the exchangeable contents of Ca, Mg, Na and K.

Because the available measurements were all after the drawdown period in which pyrite oxidation took place it is estimated the initial amounts of pyrite, exchangeable cations, reactive Al and Fe for the layer 1–3 m below ground level from the values in the deep unoxidised (3 m) soil layer. Initial solution concentrations of Cl and SO_4 were input to the model, the equilibrium concentrations of Ca, Mg, Na, K, Al, Fe and pH are calculated by the model based on the total anion concentration and the initial amounts in the soil solid phase.

Table 2 **Initial soil chemistry and pyrite oxidation parameters used in the model. SOM is soil organic matter, and Clod is the radius of the cracked clay ped (see Bronswijk *et al* 1993).**

Depth (m)	SOM %	Clay %	Pyrite %	Pyrite diam. (µm)	Clod radius (m)	Ca (meq /kg)	Mg (mmol/ kg)	K (mmol/ kg)	Na (mmol/ kg)	Al (mmol/ kg)	Fe (mmol/ kg)
0–0.1	15.4	41	0	n/a	0.1	130	140	15	25	170	90
0.1–0.5	6.4	48	0	n/a	0.1	65	140	15	40	260	90
0.5–1.0	3.0	70	0	n/a	0.25	85	140	15	40	250	90
1.0–2.0	2.6	60	1.5	5	0.35	40	160	20	100	250	90
2.0–3.0	2.6	60	1.5	5	0.35	40	160	20	100	250	90

Selective metal extractions to determine metal fractionation were also undertaken on wet samples using the methods of Claff *et al* (2011) as outlined in Table 3.

Table 3 Selective extractions used to determine solid-phase metal speciation (after Claff *et al* 2011)

Extract	Fraction	Extractant	Metal phase(s) extracted
1	Labile	1 M $MgCl_2$	Soluble species and exchangeable metal ions that may be mobilised following events such as rainfall or irrigation.
2	Acid Soluble	1 M HCl	Range of reactive minerals, including acid volatile sulfur, carbonates and a range of poorly crystalline Fe (III) minerals (eg ferrihydrite, schwertmanite less crystalline jarosite), ferrous carbonates (eg siderite) and reactive ferrous sulfides (eg machinawite). Represents the pool of metals that may be mobilised following oxidation and acidification of ASS materials.
3	Organic	0.1 M Na-pyrophosphate	Accounts for metals associated with organic matter, strongly dependent on soil type.
4	Crystalline Oxide	0.35 M acetic acid/0.2 M sodium citrate buffer with 50 g/L sodium dithionite	Metals liberated via reductive dissolution of a range of oxidised minerals associated with crystalline Fe (III) phases (egjarosite).
5	Pyritic	concentrated HNO_3	Iron and other metals associated with pyrite and other metal sulfides
6	Residual	hot acid and peroxide (USEPA Method 3050)	Accounts for that which is left following the sequential extractions above. It represents the relatively stable metals from a range of recalcitrant materials.

Oxygen diffusion and pyrite oxidation parameters

The parameters used in the pyrite oxidation model are also shown in Table 3. Pyrite was not inputted to the model in the top 1 m due to the continuous wetting and drying cycles as a consequence of normal irrigation practices and river levels in the region. There is also a higher organic content in the top layer, presumably due to inputs associated with long-term dairy farming at the site.

Pyrite crystal size was measured by Scanning Electron Microscopy (uncoated samples, low vacuum mode at 4°C under moist argon atmosphere—see Fitzpatrick *et al* 2013 for details of method). Cubic and spherical crystals were found with a diameter of approximately 5 µm (range of 1–20 µm) and some framboids of pyrite were also present (Figure 4).

Additional parameters used in the pyrite oxidation model were the Henry's law constant for oxygen (52 at 30°C), tortuosity factor (2, average value for structured soil matrices from Kristensen *et al* 2010), and the oxygen diffusion coefficient in the atmosphere (1.85 m^2/day), the oxygen diffusion coefficient in saturated soil aggregate (5 x 10^{-3} m^2/day).

For the SMASS model, the rate constant used for oxygen consumption by organic matter was 0.08 kg O_2/m^3/day from Bronswijk *et al* (1993). In the SMARTml model the oxygen consumption per kg soil organic matter is used (as indicated in the input file soil.dat in the example file provided as supplementary material) instead of kg/m^3 of soil.

We converted oxygen consumption of 0.08 kgO_2/m^3/day in Bronswijk (1993) to the 0.0008 kgO_2/kgSOM/day used in our study by assuming a SOM content in the upper part of the LMRIA soils of approximately 10% (Table 3) and a bulk density of approximately 1,000 kg/m^3 (Table 2).

The high SOM content of the LMRIA topsoil (0–50 cm, due to root decay, manure production and application) is comparable to that of Bronswijk *et al* (1993) and hence we believe oxygen consumption rates are likely comparable for the upper soil layers of our model.

However, the deep subsoil layers (>1 m) of the LMRIA has much lower SOM content (Table 3) and it is likely this is mostly comprised of rather stable/refractory organic matter. It is likely that the oxygen consumption rate by organic matter

in the deeper soils will be much lower than the upper soil. It may be preferable to use a depth dependent oxygen consumption rate but in the absence of data to confirm the above hypothesis we have currently maintained the same oxygen consumption rate through the soil profile (Table 3).

In future research the reactivity of carbon in the deeper subsoils should also be assessed to refine the oxygen consumption parameter in the model and to inform on the lability of this carbon for sulfate reduction.

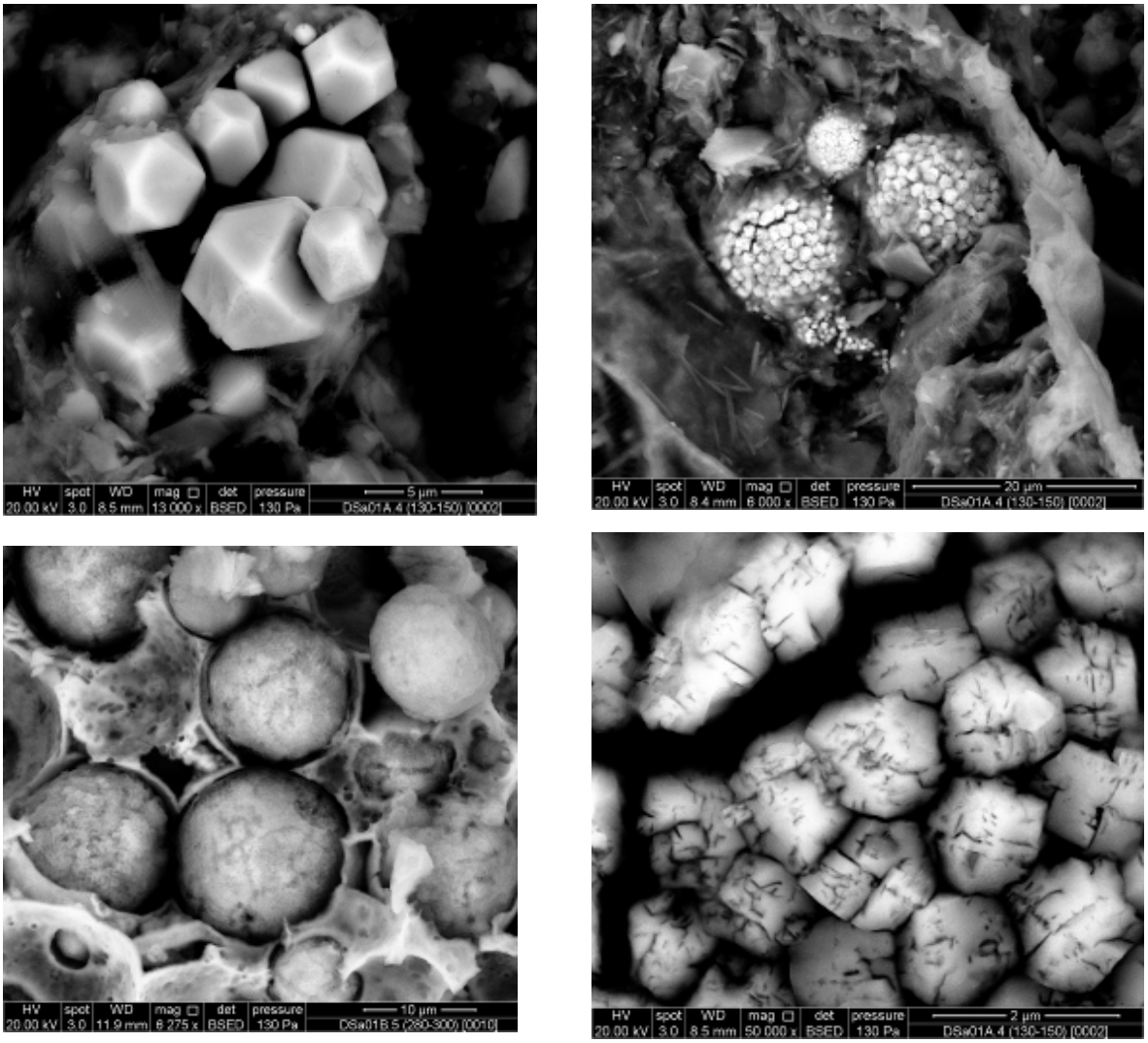

Figure 4 SEM pictures of pyrite crystals at the unoxidised lower portion of a soil core from Long Flat irrigation area. These images were used to estimate the pyrite crystal diameter (5 µm) used in the model.

Soil and solution chemistry

Groundwater data from a series of multilevel piezometers (0.5, 1, 2.5 m below ground level) was collected for approximately a one-year period and analysed for metals (Al, As, Cr, Cu, Fe, Mn, Pb, Zn), major ions (Ca, Na, Mg, Cl, SO_4), alkalinity and acidity using standard methods (APHA 2005). For further details on the groundwater monitoring program see EPA (2012).

4 Results and discussion

Water level decline and pyrite oxidation

From 2007–09 the Lower Murray River experienced a major water level decline (Figure 3) due to drought conditions and water management decisions in the Murray–Darling Basin. These were the lowest water levels measured in the region over 90 years of records. In response to the river water level decline the groundwater on the adjacent floodplain dropped nearly 1.5 m (Figure 5).

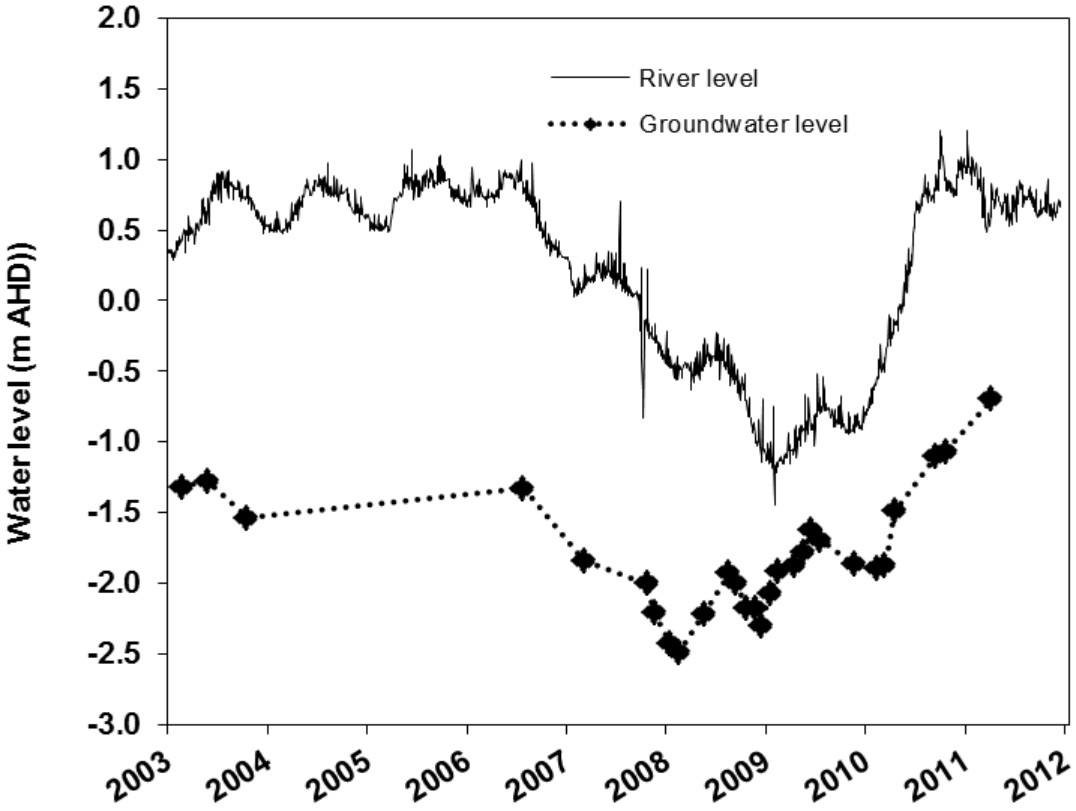

Figure 5 Measured river (Murray Bridge) and groundwater (Mobilong 01A site) levels

As a consequence, the clay soils dried and cracked, and the soil desaturated exposing the pyrite in the deeper (ie predominantly in the 1–2.5 m bgl zone) subsoil layers to oxygen, likely for the first time in decades or centuries for the deeper layers below mean sea level (eg see conceptual models in Fitzpatrick *et al* 2013). Figure 6 illustrates the Hydrus-1D outputs for water content showing this desaturation.

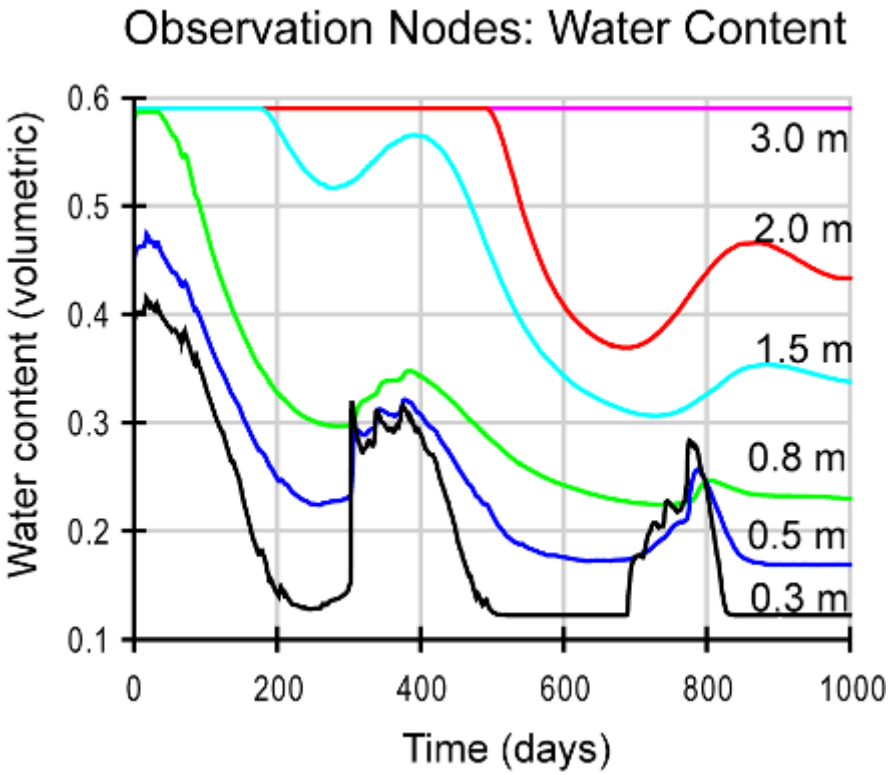

Figure 6 Modelled soil water content from Hydrus-1D during decline of river and groundwater levels from 2007–09

The pyrite oxidation model inputs (t=0) and outputs are shown in Figure 7 in comparison to measured data on 1 March 2011. The model successfully predicted the loss/oxidation of pyrite from the soil layer between 1–3 m below ground level. The acid-base accounting results in comparison with earlier results (Fitzpatrick *et al* 2013) are also shown in Figure 7. The main noticeable change is a loss in the retained acidity (jarosite) fraction. This may be due to dissolution of the jarosite following the multiple irrigation events at the site.

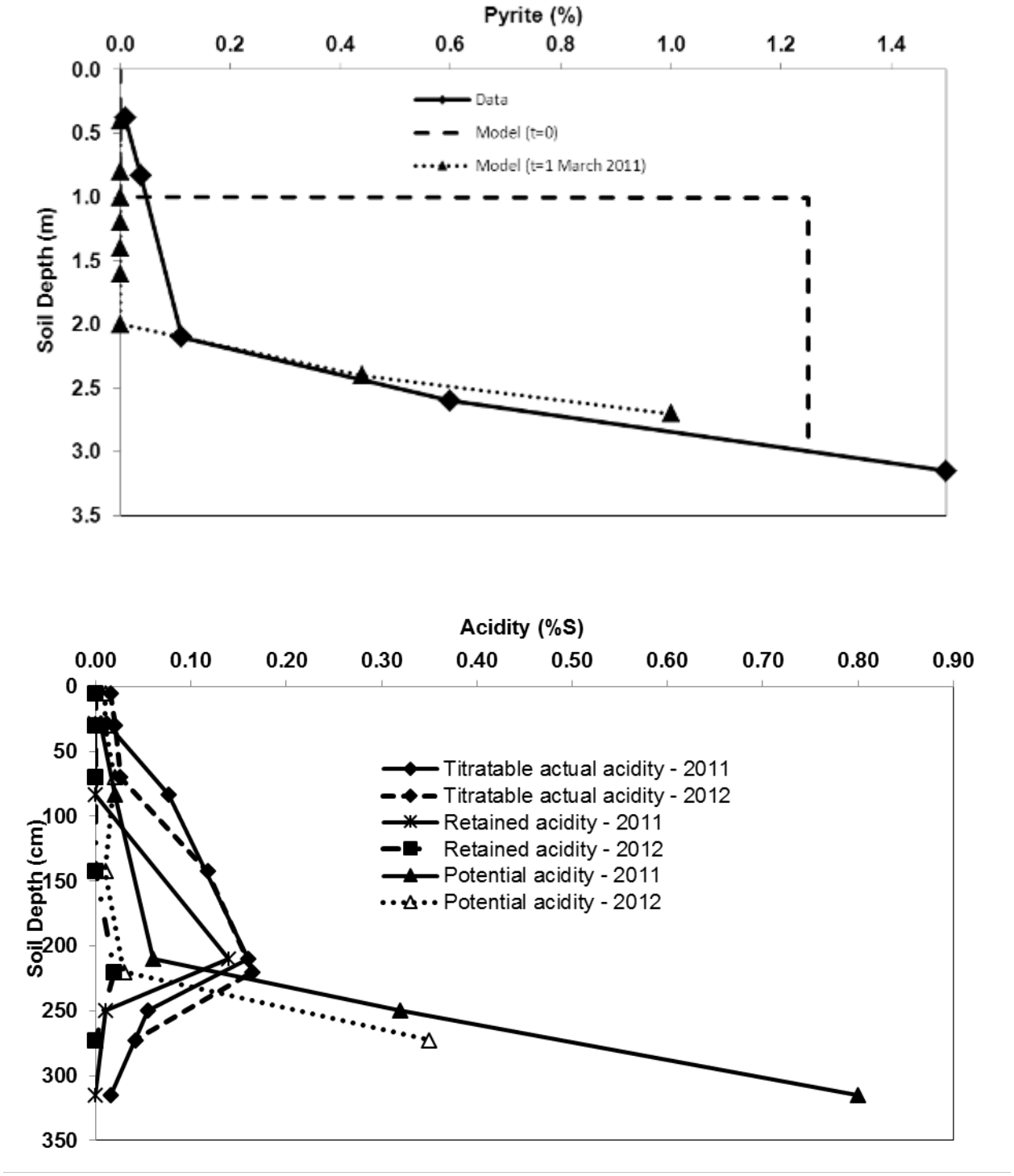

Figure 7 **Modelled and measured pyrite oxidation (top), and measured (from 2011 and 2012 sampling) acid-base soil analysis results (bottom)**

Sensitivity tests were also performed on the pyrite oxidation model for the parameters that were not measured, specifically the pyrite diameter, oxygen diffusion coefficient in the saturated soil matrix, the oxygen consumption by organic matter, and the tortuosity factor. The results are shown in Figure 8 with the most sensitive parameter the oxygen diffusion coefficient, followed by the tortuosity factor, pyrite diameter, and the oxygen consumption rate by organic matter.

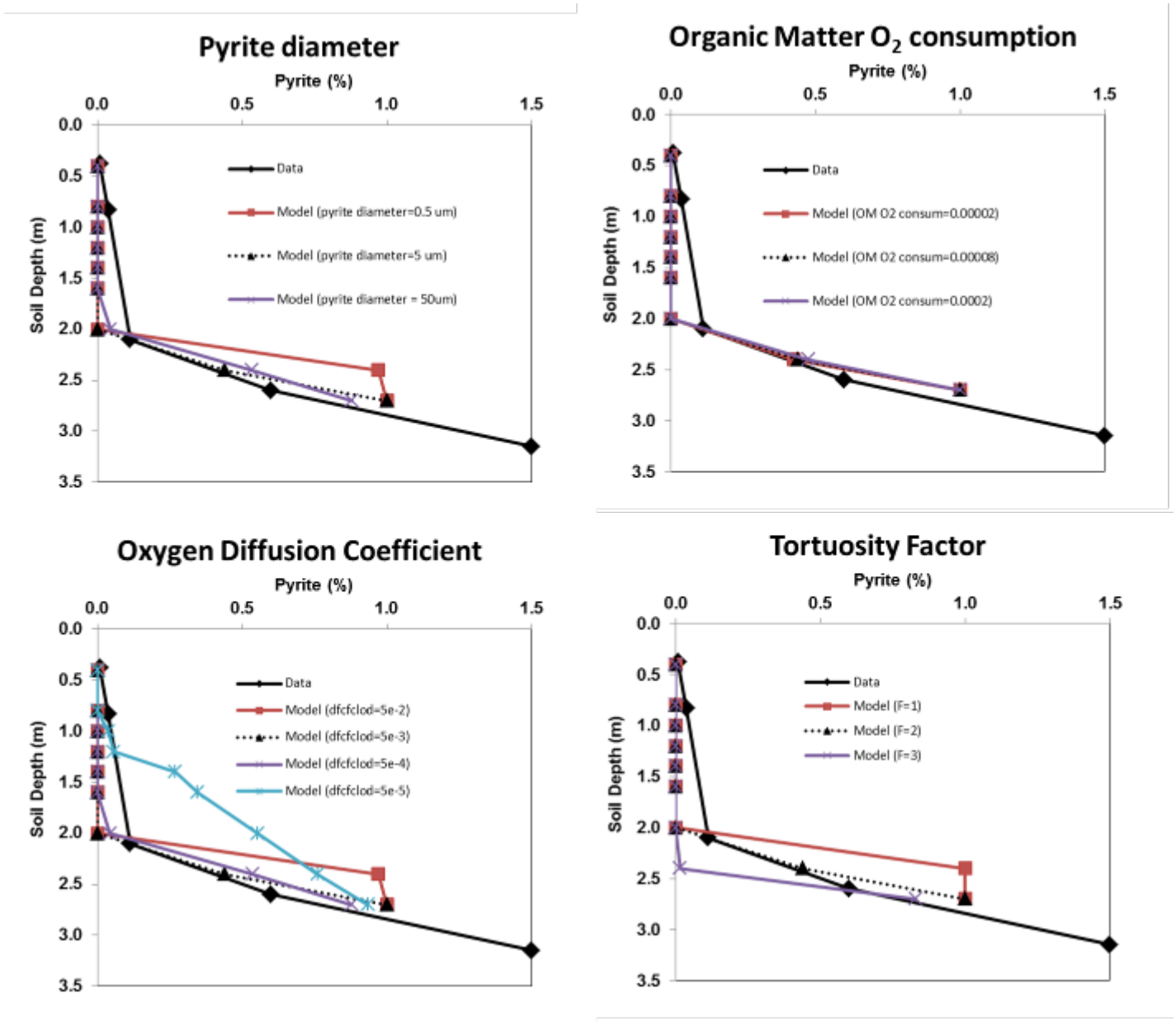

Figure 8 **Sensitivity tests for various pyrite oxidation parameters (pyrite diameter in µm, oxygen consumption by organic matter in $kgO_2/m^3/day$, oxygen diffusion coefficient in m^2/day, and the dimensionless tortuosity factor) in comparison to measured data**

The pyrite oxidation resulted in low pH (pH<4.5) in the 1–2.5 m bgl soil layer, a loss of soil cation exchange capacity, and replacement of the original cations (Ca, Mg, Na, K) on the clay exchange sites with acidic cations (Al^{3+}, H^+) [Figure 9].

The model represented the measured pH quite well after five years of simulation, although the deeper layer is predicted to be acidic in the model at this time which was not observed. This may be an artifact of the simplified Hydrus-1D bottom boundary condition that is not representing the more complex drainage hydrology adequately. Further investigation and Hydrus 2D/3D modeling would be required to better understand the hydrological processes at the site.

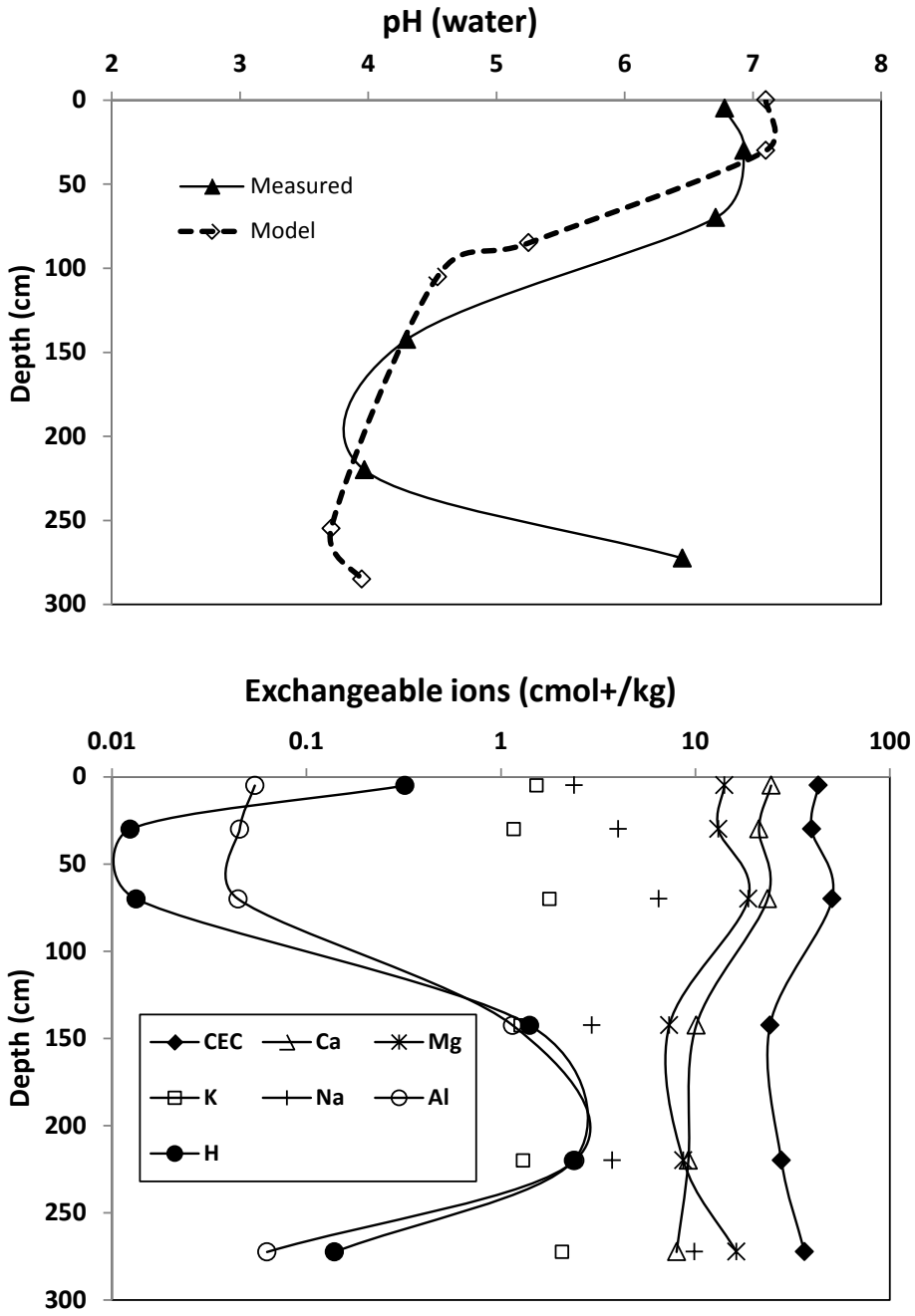

Figure 9 **Soil pH (measured and modeled) and measured cation exchange capacity (exchangeable Ca, Mg, K, Na, Al, H and the total cation exchange capacity, CEC) after 1,850 days**

The results from the sequential extraction analyses are shown in Figure 10. In the most acidic layer (1–2.5 m bgl) a large peak in the amount of Al, As and Mn in the exchangeable (labile) fraction was observed. A large amount of Fe and Al was also associated with the reactive (acid soluble) and organic fractions in the upper soil profile. A loss of Fe and some other metals from the pyritic fraction was observed in agreement with the independently measured (via chromium reducible sulfur method) pyrite profile (Figure 7). All exchangeable metal fraction values are below interim sediment quality guidelines (Simpson *et al* 2005) although no guideline existed for Al.

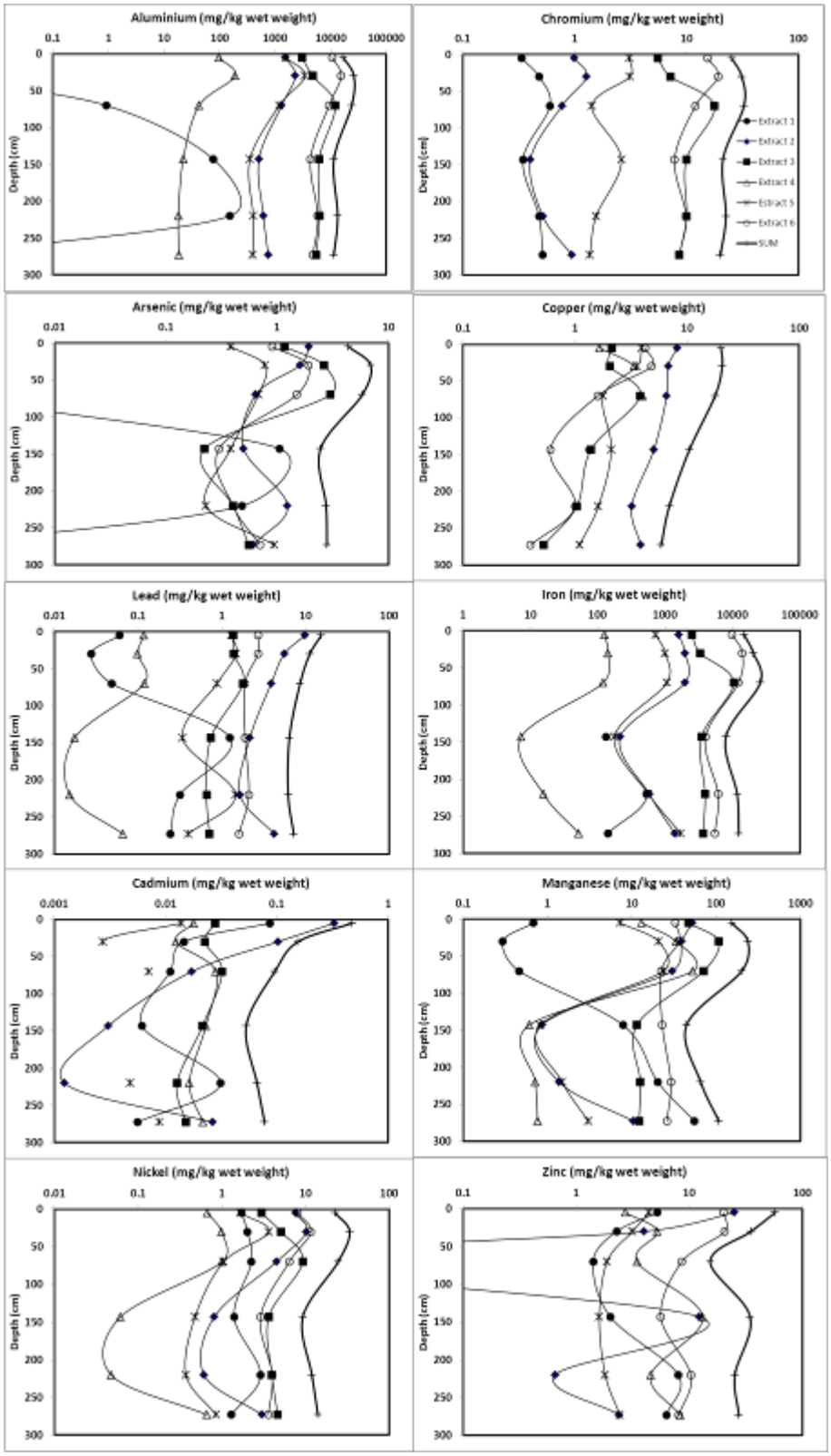

Figure 10 Metal speciation in the soil (see methods section for extract description)

Figure 11 shows the change over time of pH together with the amounts of Al and Fe-hydroxide and jarosites for the soil at 1.2–1.3 m bgl. In this layer initially present pyrite was rapidly oxidised during the drawdown of the water table. Initially the pH declines very rapidly from pH 7.2 to 5.2, although the produced acid is mainly buffered by exchange of base cations (Ca^{2+}, Mg^{2+}) with H^{+} and Al^{3+}. At pH 5.2 $Al(OH)_3$ starts to dissolve, and the $Al(OH)_3$ buffering system keeps the pH just below pH 4. If $Al(OH)_3$ would be depleted the pH easily drops to values as low as pH 2.5. Together with the oxidation of pyrite, K- jarosite is formed at the expense of ferric oxide ($Fe(OH)_3$).

The formation of K-jarosite is limited by the amount of potassium in the soil. Because initial amounts of K in the soil were not large enough to produce the amount of jarosite as was estimated from measurements with the acid-base accounting

suite, we also included Na-jarositein the model. The model simulations (Figure 11) shows that once all K is used in the formation of jarosite, Na-jarosite starts to form. Figure 11 also shows that upon groundwater level recovery and soil rewetting (days >1,000), pH starts to rise somewhat. However, the dissolution of jarosite (first Na-jarosite starts to dissolve) brings acidity into solution. The dissolution of jarosite is also suggested by measurements, which show a decrease in retained acidity in 2012 compared with measurements in 2011 (Figure 7).

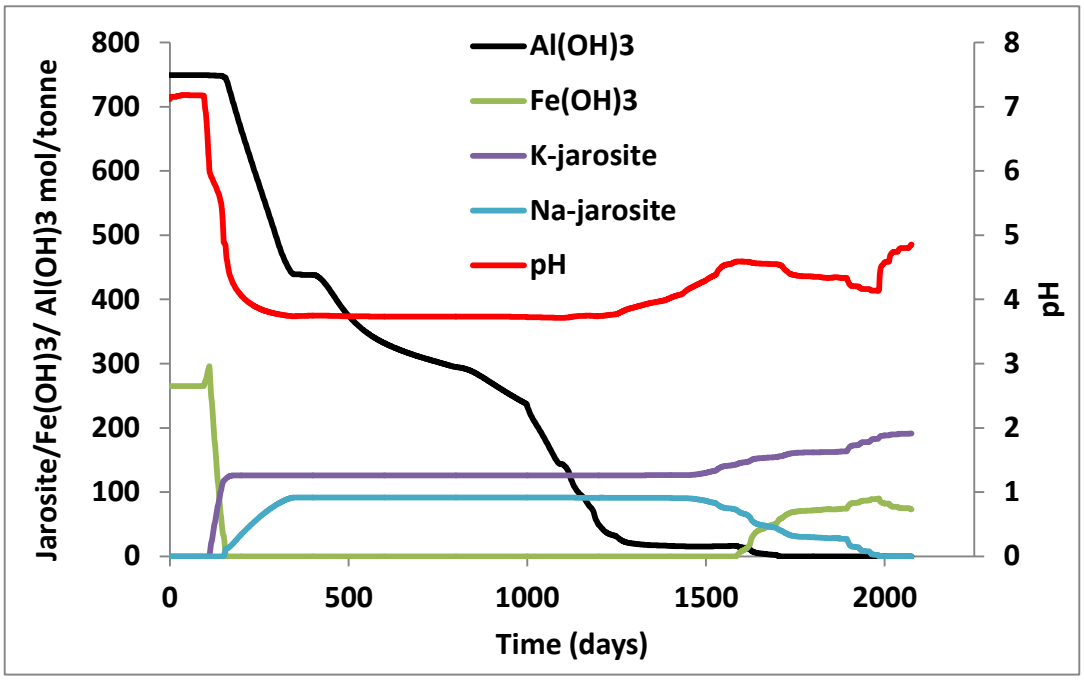

Figure 11 **Model predictions for the amounts of aluminium-hydroxide, ferric hydroxide, K-jarosite, Na-jarosite and the change overtime of the pH at 1.2–1.3 m bgl as a result of pyrite oxidation during the drawdown of the water table (day 0–1,000), the rewetting of the soil profile due to recovery of the groundwater level (day 1,000–1,880), and leaching of acidity by recommencement or irrigation and drainage (approx. day >1,881)**

Rewetting and drainage of acidity

The rewetting of the oxidised soil profile occurred in late 2010 when the river returned to normal pool levels (Figure 3). The modeled and measured results for hydraulic head associated with irrigation and drainage at the Long Flat irrigation area after irrigation recommenced in 2011 are shown in Figure 12. The model represented the measured data well, particularly considering the simplified Hydrus-1D model representation of the horizontal drain boundary conditions at the site.

The model also represented the measured conservative solute (chloride) concentration trends well, with dilution and flushing observed over time (Figure 13). Aluminium showed similar trends to chloride (Figure 13) which indicates that irrigation-induced flushing is an important mechanism that reduces groundwater metal concentrations. However this flushing process also results in metal export to drainage channels and to the river.

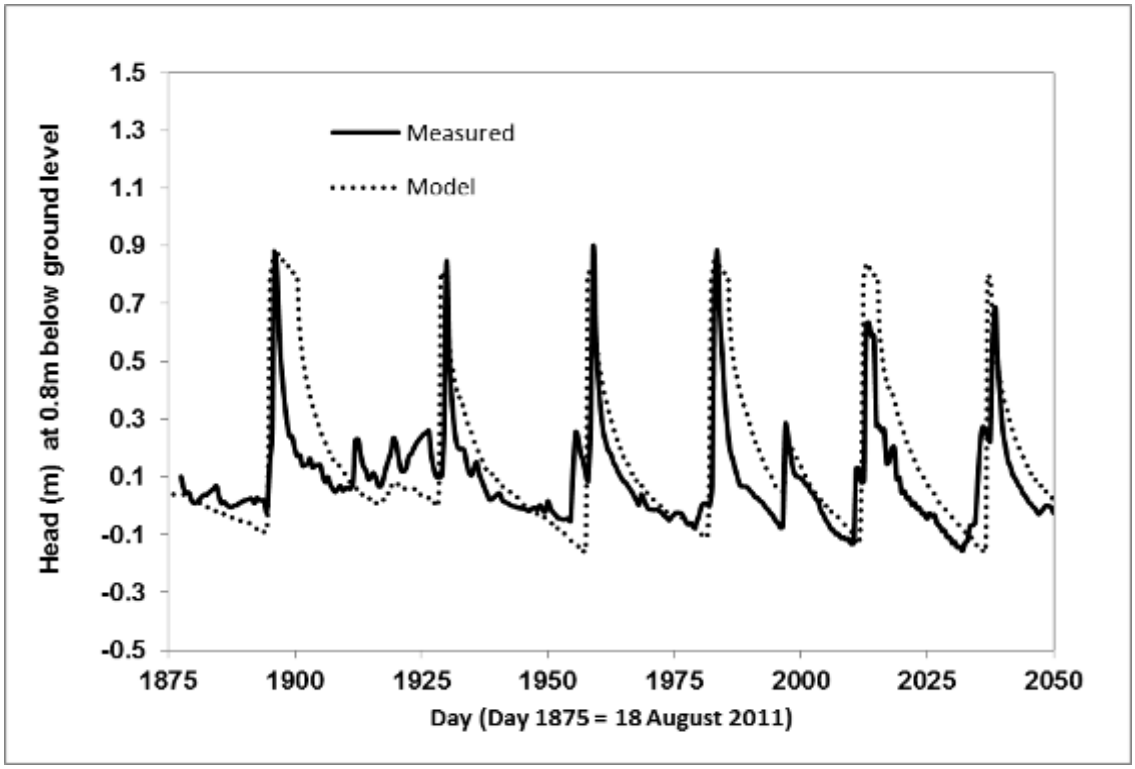

Figure 12 Modeled and measured hydraulic head (at 0.8 m bgl)

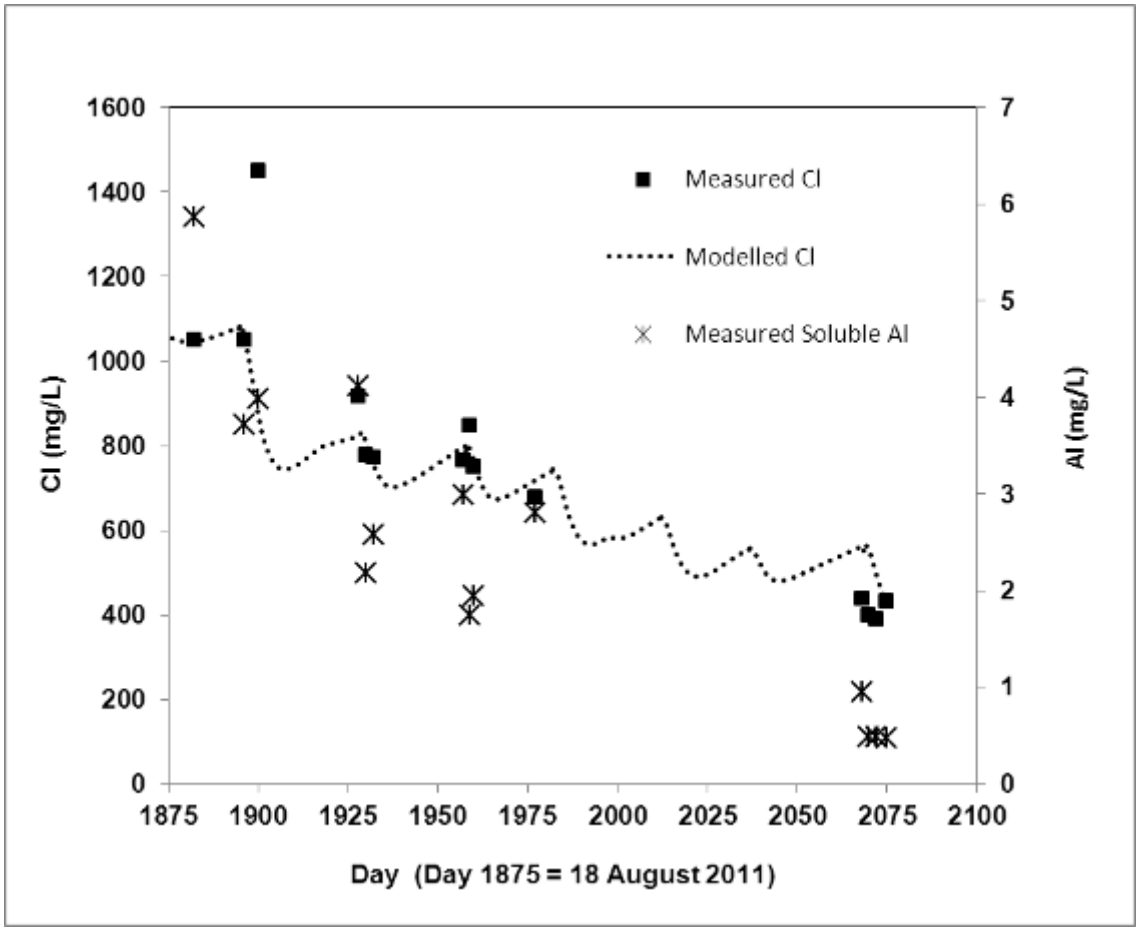

Figure 13 Modeled and measured Cl and measured soluble Al concentrations in response to rainfall and irrigation

Metal solubility

The oxidation of pyrite and acidification strongly influences the concentrations of potential toxic trace metals in soil. SMARTml can simulate these changes in metal solubility using the geochemical (sub) model ORCHESTRA (Bonten *et al* 2009, Groenenberg *et al* 2012). Because metal contents in soil before the drawdown of the water table were not available, trace metals were not included in the dynamic simulation with the model. However, to be able to test the model under extreme conditions prevailing in acid sulfate soils we evaluated the model by comparing predicted solution concentrations with measurements from the 2012 sampling. Solution concentrations were predicted from measured metal contents in the solid phase and soil properties. The reactive solid phase metal content was measured with the sequential extraction (sum of 1 M $MgCl_2$ and 1 M HCl extracts). Other important inputs measured were pH and DOC, the organic carbon and clay content and contents of Al and Fe oxides (sum of 1 M $MgCl_2$, 1 M HCl and pyrophosphate extracts in the sequential extraction) from measurements in April 2012.

The measured versus modeled trace metal concentrations results are shown in Figure 14. The model and measured results agree well for most metals over a wide concentration range. Concentrations of Ni and Zn appear to be high in this soil and might have toxic effects. The results support the findings of Bonten *et al* (2011) and Groenenberg *et al* (2012) on the usefulness of multi-surface reactive models which require no specific calibration (just the soil reactive metal content, amount of Al and Fe oxides and organic matter, and concentration of DOC and major ions in pore water). However, the model overestimates the Pb concentration and underestimates the Cu concentration and the reasons for this are unclear at present.

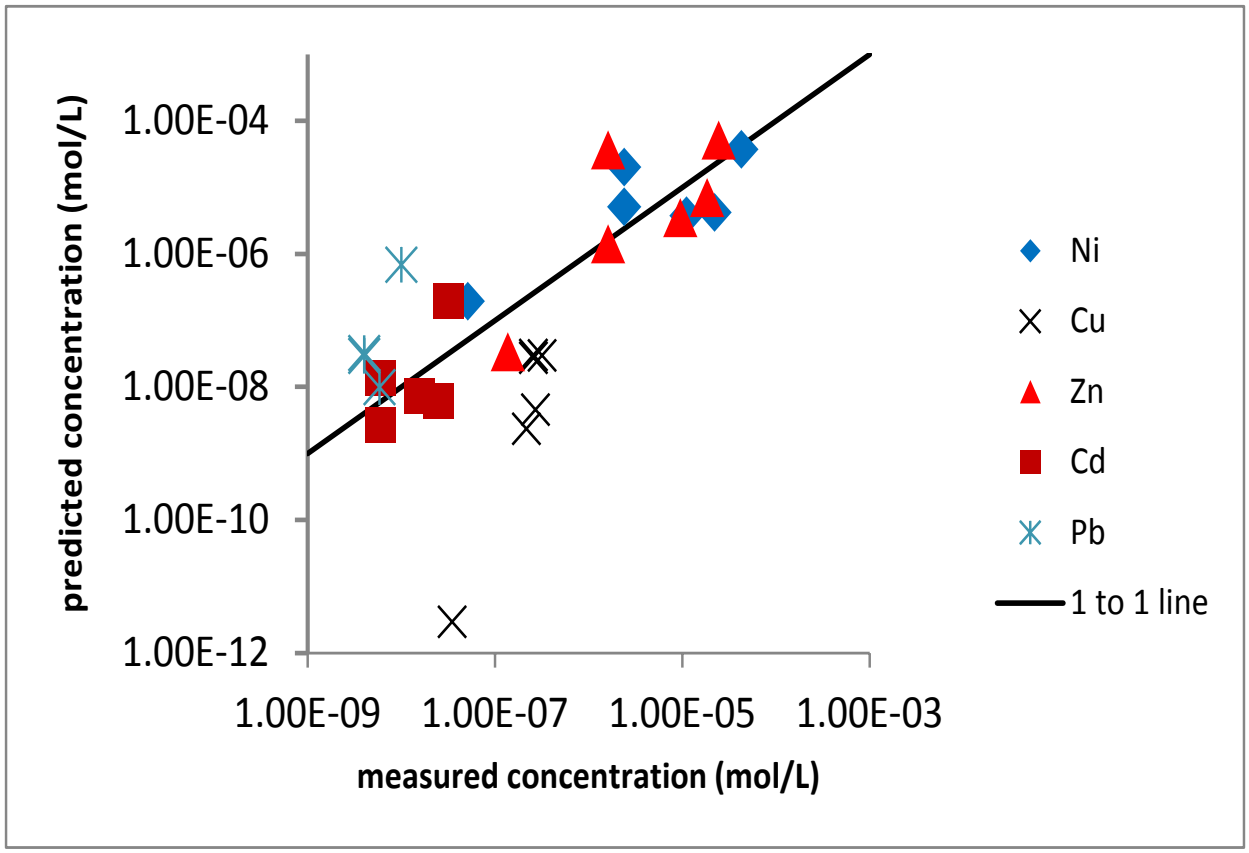

Figure 14 Measured and predicted equilibrium concentrations in solution (based on present metal contents in soil)

Management implications

A management scenario was run in the model where the groundwater level corresponding to a river level of approximately 0.5 m AHD was stabilised and two environmental land management allocation (ELMA, available to irrigators in the LMRIA) irrigations performed per year. The 0.5-m river level relates to the downstream Murray–Darling Basin Plan target for the Lower Lakes of 0.4 m AHD and is a level sufficient to gravity fed flood irrigation. In this scenario a much smaller soil acidification hazard is predicted to form compared to the actual situation of water levels falling to

approximately –1 m AHD (Figure 15). This is due to the maintenance of a higher water table and more saturated conditions under the floodplain where the acid sulfate soils are located.

River level appears to be much more important than irrigation in maintaining groundwater levels and soil saturation. However during drought, irrigation would undoubtedly also provide soil benefits and reduce acid sulfate soil impacts. Additional modelling using a 2/3D model to couple river level to groundwater level under the floodplain would be worthwhile to refine the management outcomes.

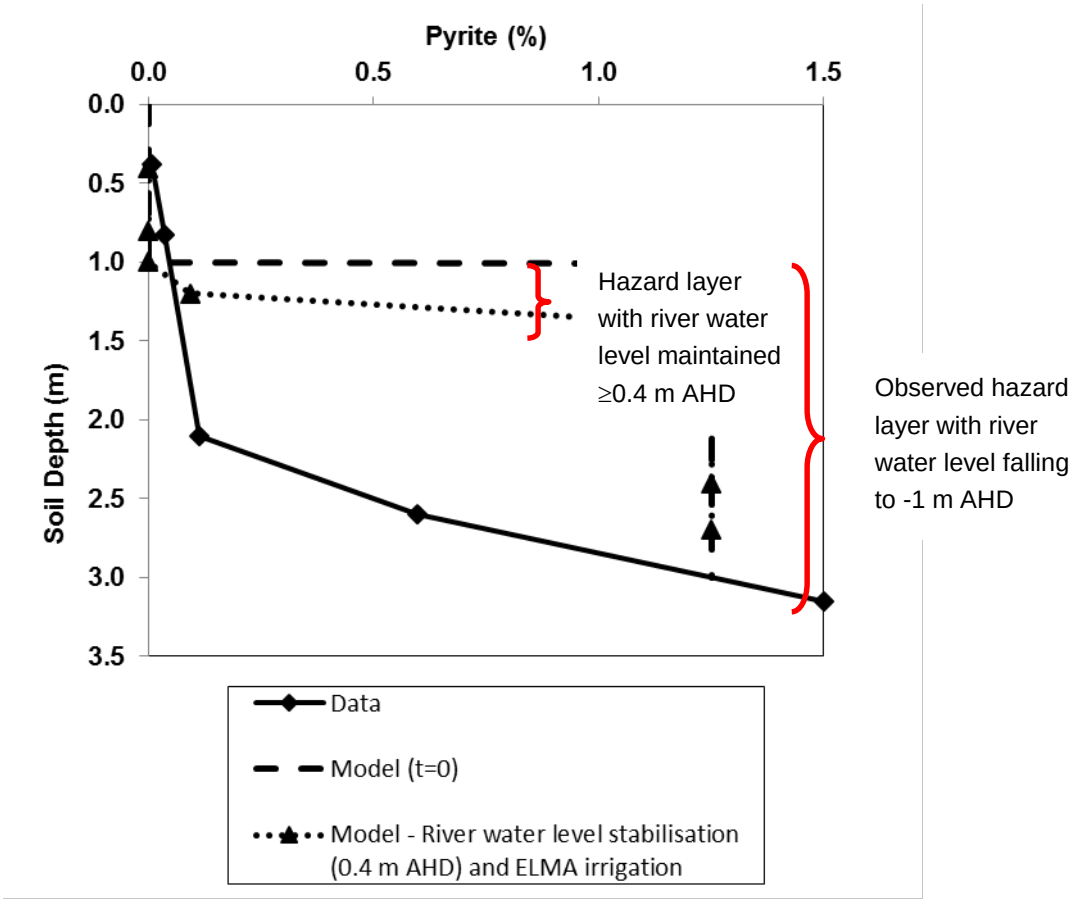

Figure 15 **Management scenario showing how soil pyrite oxidation could potentially be minimised by stabilisation of river levels at 0.5 m AHD and use of two environmental (ELMA) irrigations**

5 Conclusions

The existing SMARTml model has been revised to include a pyrite oxidation model and successfully coupled to Hydrus-1D. This model can be used to simulate pyrite oxidation and other complex biogeochemical processes in acid sulfate soils. The pyrite oxidation model was successfully developed and tested in the Lower Murray Reclaimed Irrigation Area (LMRIA).

Measured soil physical properties were used to parameterise a Hydrus-1D model. The model was calibrated and successfully represented current wetting and drying cycles at the site. Regional groundwater data was used to simulate the falling water table under the LMRIA during the 2007–09 drought in Hydrus-1D. The predicted water contents decreased markedly during drought and indicated soil drying would occur to a depth of up to 3 m below ground level. This is consistent with the observed oxidised zone of sulfuric material (pH<4) and reactive metal fractions in the deep LMRIA subsoil layers.

The soil pH profile and depth of pyrite oxidation was successfully simulated in SMARTml over a 1,850-day period. The model also successfully represented the flushing of solutes from the soil profile and solution metal concentrations. The refined model now provides a useful management tool for assessing and managing impacts from acid sulfate soils.

For the LMRIA, preliminary management scenarios demonstrated how maintaining desirable river levels (>0.5 m AHD corresponding to >0.4 m AHD guideline downstream in the Lower Lakes under the Murray–Darling Basin Plan) is critical to preventing oxidation of hypersulfidic material (ie pyrite-rich layers) in acid sulfate soils.

Further testing and development of SMARTml (to include sulfate reduction) would be beneficial. The reactivity of carbon in the deeper subsoil layers should also be assessed to refine the oxygen consumption parameter in the model and to inform on the lability of this carbon for sulfate reduction. Additional modeling using a 2D model to couple river level to groundwater level under the floodplain would also be worthwhile to refine the management outcomes.

6 Acknowledgements

The funding of the Murray–Darling Basin Authority and support provided by Rob Kingham are gratefully acknowledged. The assistance of Rob Frazer (soil coring), and David Palmer and Emily Leyden (EPA) with the project is also kindly acknowledged.

7 References

Ahern, CR, McElnea AE and Sullivan LA 2004, *Acid Sulfate Soils Laboratory Methods Guidelines*, QLD DNRME.

Bonten LTC, Groenenberg JE, Meesenburg H and de Vries W 2011, 'Using advanced surface complexation models for modelling soil chemistry under forests: Solling Forest, Germany', *Environmental Pollution* **159**:2831–2839.

Bronswijk J and Groenenberg JE 1992 'A simulation model for acid sulfate soils: I basic principles, in Dent D and M van Mensvoort (eds), *Selected papers of the Ho Chi Minh City Symposium on Acid Sulfate Soils*, ILRI Publication 53, IlRI: Wageningen, viewed 10 December 2013, http://content.alterra.wur.nl/Internet/webdocs/ilri-publicaties/publicaties/Pub53/pub53-h17.pdf

Bronswijk JJE, Nugroho K, Aribawa IB, Groenenberg JE and Ritsema CJ 1993, 'Modeling of Oxygen Transport and Pyrite Oxidation in Acid Sulphate Soils', *J Enviro Qual,* **22**:544–554.

Claff SR, Burton ED, Sullivan LA and Bush RT 2011, 'Metal partitioning dynamics during the oxidation and acidification on sulfidic soil', *Chemical Geology*, **286**:146–157.

Dzombak DA and Morel FMM 1990, *Surface complexation modeling: Hydrous Ferric Oxide*, Wiley, New York.

Dent DL and Pons LJ 1995, 'A world perspective on acid sulfate soils', *Geoderma*, **67**:263–276.

EPA 2012, *Lower Murray River Irrigated Area Acidification Risk Project: Preliminary monitoring report 2011–12,* Environment Protection Authority, Adelaide, viewed 10 December 2013, www.epa.sa.gov.au/xstd_files/Water/Report/Preliminary%20Report_LMRIA_Final.pdf

Fitzpatrick RW, Shand P, Simpson S, Grocke S, Raven M, Baker AKM ,Mosley L and Self PG 2013, *Assessment of re-flooded acid sulfate soil environments at Long Flat, Jervois, Toora and Pompoota in the Lower Murray Reclaimed Irrigation Area (LMRIA)*,CSIRO Land and Water Science Report No 03/2012, 220 pp.

Klute A 1986, *Methods of Soil Analysis, Part 1*, Agronomy Monogram 9 (2nd ed), American Soc. of Agronomy, 1188 pp.

Groenenberg JE, Dijkstra JJ, Bonten LTC, de Vries W and Comans RNJ 2012, 'Evaluation of the performance and limitations of empirical regression models and process based multi-surface models to predict trace element solubility in soils', *Environmental Pollution*, **168**:98–107.

Hiemstra T and van Riemsdijk WH 2006, 'Biogeochemical speciation of Fe in ocean water', *Marine Chemistry*, **102**:181–197.

Kinniburgh DG, van Riemsdijk WH, Koopal LK, Borkovec M, Benedetti MF and Avena MJ 1999, 'Ion binding to natural organic matter: Competition, heterogeneity, stoichiometry and thermodynamic consistency', *Colloids and Surfaces A: Physicochemical and Engineering Aspects,* **151**:147–166.

Kristensen AH, Thorbjørn A, Jensen MP, Pedersen M and Moldrup P 2010, 'Gas-phase diffusivity and tortuosity of structured soils', *Journal of Contaminant Hydrology*, **115**:26–33

Milne CJ, Kinniburgh DG, van Riemsdijk WH and Tipping E 2003, 'Generic NICA-Donnan model parameters for metal-ion binding by humic substances', *Environmental Science and Technology*, **37**:958–971.

Rawls WJ and Brakensiek DL 1985, 'Prediction of soil water properties for hydrologic modelling', in Jones E and Ward TJ (eds), *Watershed Management in the Eighties*, Proc. Symp. Irrig. Drain. Div. ASCE, Denver, CO/ASCE, New York.

Pons LJ 1973, 'Outline of the genesis, characteristics, classification and improvement of acid sulphate soils', in Dost H (ed), *Proceedings of the 1972 (Wageningen, Netherlands) International Acid Sulphate Soils Symposium, Volume 1*, International Land Reclamation Institute Publication 18, Wageningen, Netherlands, pp 3–27.

Šimůnek J, Šejna M, Saito H, Sakai M and van Genuchten MTh 2008, *The Hydrus-1D Software Package for Simulating the Movement of Water, Heat, and Multiple Solutes in Variably Saturated Media, Version 4.0*, HYDRUS Software Series 3, Department of Environmental Sciences, University of California Riverside, Riverside, California, USA, viewed 10 December 2013, www.pc-progress.com/en/Default.aspx?hydrus-1d

Simpson SL, Batley GE, Chariton AA, Stauber JL, King CK, Chapman JC, Hyne R, Gale SA, Roach AC and Maher WA 2005, *Handbook for Sediment Quality Assessment*, CSIRO, Bangor NSW, 117 pp, viewed 10 December 2013, www.csiro.au/files/files/p8m1.pdf

Wunderly MD, Blowes DW, Frind EO and Ptacek CJ 1996, 'Sulfide mineral oxidation and subsequent reactive transport of oxidation products in mine tailings impoundments: A numerical model', *Water Resources Research*, **32**:3173–3187.